Journal of CO2 Utilization 84 (2024) 102859

Contents lists available at ScienceDirect

Journal of CO2 Utilization

journal homepage: www.elsevier.com/locate/jcou

Novel utilization of waste concrete powder in alkali-activated binder

Aidarus Yonis [a,1], Prabhat Vashistha [a,1], Yanchen Oinam [a], Martin Cyr [b], Sukhoon Pyo [a,*]

[a] Department of Civil, Urban, Earth, and Environmental Engineering, Ulsan National Institute of Science and Technology (UNIST), 50 UNIST-gil, Ulju-gun, Ulsan 44919, Republic of Korea

[b] Laboratoire Matériaux et Durabilité des Constructions (LMDC), INSAT/UPS Génie Civil, 135 Avenue de Rangueil, 31077 Toulouse Cedex 04 France

ARTICLE INFO

Keywords:
Waste concrete powder
Alkali-activated binder
Mineralogical analysis
Hydration analysis
LCA analysis

ABSTRACT

This experimental study investigates a novel approach to utilize waste concrete powder (WCP) in conjunction with metakaolin as a precursor in the production of alkali-activated binder for sustainable consumption of construction and demolition waste. A Chapelle test confirms the presence of reactive silica in thermo-mechanically activated WCP. Different alkali-activated mixtures with metakaolin replacement ranging from 0 % to 80 % were prepared. The mixture with 40 % activated WCP, with a sodium silicate to sodium hydroxide ratio of 2, achieved better compressive strength than the reference sample without WCP. Mineralogical analysis of the mixture pastes revealed that activated WCP-based mixtures developed geopolymer gel and C-S-H gel, contributing to better strength properties in the case of the mixture with 40 % activated WCP. Life cycle analysis demonstrated that incorporating 40 % thermo-mechanically activated WCP by replacing metakaolin reduces carbon dioxide emissions by 49.5 % and 2.2 % compared to Portland cement and metakaolin-based binder, respectively.

1. Introduction

Concrete stands as a pervasive construction material, employed globally with an annual production exceeding 10 billion tons [1,2]. Despite its durability and versatility, the environmental impact of cement, a pivotal concrete component, cannot be overlooked [3–5]. The production of cement not only requires substantial energy but also represents a significant source of greenhouse gas emissions. With the escalating demand for cement, an immediate imperative exists to discover sustainable approaches that mitigate its environmental footprint. Conversely, the realm of construction and demolition (C&D) waste represents a substantial global source of waste, marked by a continual surge in generation and volume propelled by urbanization and infrastructure expansion. As per the United Nations Environment Programme (UNEP) report, global waste generation reached approximately 2.01 billion tons in 2016. Projections indicate a rise to 2.2 billion tons by 2025 and a further increase to 2.7 billion tons by 2050, while C&D accounts for a range from 30 % to 44 % of the total waste generated globally [6,7]. Efficient handling of C&D waste stands as a crucial imperative to mitigate its environmental impact and foster sustainable practices. Addressing the escalating quantities of C&D waste produced on a global scale requires innovative solutions. One such impactful strategy involves recycling this waste to produce high-quality aggregate. However, it's noteworthy that the production process of recycled aggregate introduces a by-product known as waste concrete powder (WCP). Fig. 1 represents the concrete recycling life cycle and the WCP generation process. Comprising predominantly fine particles, WCP is conventionally treated as inert waste and consigned to landfills in common waste disposal practices [8–10]. Notably, WCP is rich in minerals like quartz and calcite, housing hydrated cement as well. With a substantial ranging between 80 % and 95 % of calcium and silica content, WCP presents a unique opportunity for exploration and utilization [11–13]. Based on the mineralogical composition of the WCP, several studies suggested that it is utilization as an inert material in concrete applications [8,14,15]. However, recognizing the environmental impact of this waste, many researchers also directed their focus towards innovative approaches to incorporate WCP as a binding material [12].

Earlier research proposed the clinkering method as an efficient means of reusing concrete waste into a supplementary binder. However, the sustainability of this method is marred by its substantial carbon emission due to the use of cement with WCP [12,16–19]. An eco-friendly alternative is the treatment of waste concrete by using alkali activators.

* Corresponding author.
E-mail address: shpyo@unist.ac.kr (S. Pyo).
[1] These authors contributed equally to the present study

https://doi.org/10.1016/j.jcou.2024.102859
Received 19 April 2024; Received in revised form 26 June 2024; Accepted 26 June 2024
Available online 29 June 2024

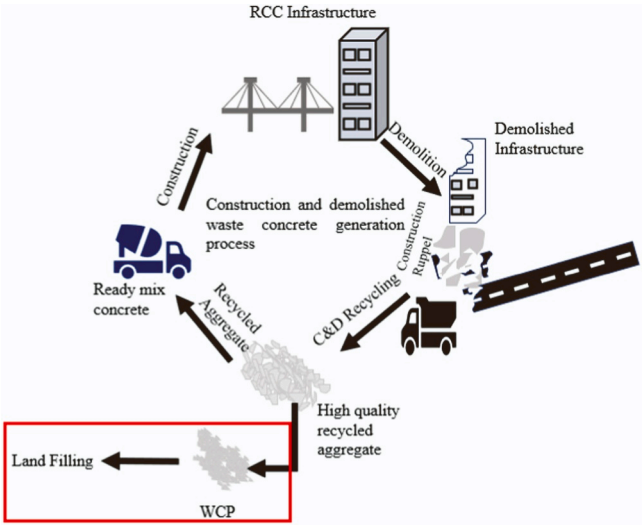

Fig. 1. Lifecycle of concrete and WCP generation process.

Typically composed of SiO_2, CaO, Al_2O_3, Fe_2O, and MgO, waste concrete provides essential precursors for producing alkali-activated binders [20,21]. The hydrated cement within waste concrete predominantly contains phases like calcium hydroxide, calcite, and calcium silicate hydrate (C-S-H) [11,16,22]. Moreover, mineral compositions from the aggregate in the original concrete, such as anorthite $Ca(Al_2Si_2O_8)$, poorly crystalline silica, and amorphous silica, function as a calcium-aluminosilicate source for the alkali solution in a sodium hydroxide environment. These compositions have demonstrated phase transformation reactivity in earlier research [23]. This suggests the potential for complete recycling of waste concrete.

An earlier study by Abdel-Gawwad et al. [24] explored the alkali-activation of WCP and sludge contained with lead. Notably, the mechanical performance was improved with the addition of this sludge up to 10 % in NaOH treated concrete waste. The alkali activation resulted in the dissolution of calcium silicate minerals such as alite, which leads to the acceleration of the hydration, and also changes the structure of the C-S-H to sodium calcium silicate hydrate (N-(C)-S-H) [24–26]. In another study, a thermal treatment of waste concrete combined with various percentage of NaOH pellets was investigated at a temperature of 1100 °C and 1200 °C for a duration of two hours by Abdel-Gawwad et al.[27]. This resulted in the generation of an amorphous phase from the crystalline phase, demonstrating potential with acceptable strength upon water addition. Chen et al. [28] also discovered that using a NaOH solution as an activator in a geopolymer system along with WCP resulted in the complete dissolution of portlandite, leading to the formation of amorphous C-(A)-S-H. However, previous studies focused on higher energy treated methods, laboratory fabricated WCP, and overlooked the influence of the alkali proportion on the WCP to aluminosilicate precursor binder.

While these findings underscore the potential of alkali activation for waste concrete recycling, crucial parameters such as molarity of the NaOH, Na_2SiO_3 to NaOH ratio, and application of WCP with metakaolin as a precursor remain unexplored for optimal cementitious properties. Notably, while metakaolin is a common precursor for alkali-activated binders, its specific effects on application with WCP have not been thoroughly studied. Therefore, this study aims to tackle this gap by investigating the impact of various proportions of WCP on the alkali-activated binder. The utilization of alkali-activated cementless binders also presents a novel avenue for the valorisation of WCP, offering a sustainable solution for the manufacturing of alternative cement. To assess the reactivity of alkali-activated binder, a comprehensive array of chemical and mineralogical techniques was deployed, encompassing the Chapelle test, X-ray fluorescence (XRF), Fourier transform infrared (FTIR), mercury intrusion porosimetry (MIP), X-ray diffraction (XRD), isothermal calorimetry, and differential thermal analysis/thermogravimetry (DTA/TG). These methods were strategically designed as an initial exploration to pave the way for subsequent investigations into the mechanical performance of the samples. In addition to the intricate analysis of reactivity, a lifecycle assessment (LCA) was conducted to scrutinize the effect of activated WCP based binder on the environment. This LCA involved the integration of experimental protocols to quantitatively measure the environmental implications of various mixture formulations. This comprehensive approach seeks to provide a holistic understanding of the chemical and environmental aspects, laying the foundation for a more thorough exploration of activated WCP's effects on the mechanical attributes of cement mixes. This approach aligns with the broader industry trend of seeking environmentally friendly alternatives to reduce the ecological footprint associated with traditional concrete production. In essence, the research not only addresses the issue of managing waste generated during aggregate production but also explores a promising pathway towards more sustainable practices in the construction materials sector.

2. Materials and experimental program

2.1. Materials

The WCP was gathered from the municipal recycling plant in Ulsan, South Korea. To determine the oxide composition of the WCP, burned and milled WCP (BMWCP) at 650°C for 2 hours, and metakaolin (MK), XRF analysis was conducted, and the results are presented in Table 1. The analysis revealed that the WCP contained significant amounts of silicon dioxide (SiO_2), aluminium oxide (Al_2O_3), and calcium oxide (CaO), accounting for approximately 60 % of the composition. The presence of amorphous SiO_2 and CaO is beneficial for using WCP as an alkali-activated precursor material. However, it should be noted that accurately quantifying the amount of sand present in the WCP was challenging. In addition to SiO_2 and CaO, the WCP contained notable amounts of magnesium oxide, potassium oxide (K_2O), sulfur trioxide (SO_3), and titanium dioxide (TiO_2), which is believed to be from the parental crushed aggregate during the recycling process [29]. Exhibiting a 15 % of loss on ignition (LOI) in WCP indicates the presence of calcium carbonates and organic impurities like asphalt, which can be seen in the raw material. Overall, this information highlights the oxide composition of the WCP utilized in this study.

2.2. Experimental program

The procedure for preparing activated WCP was adapted from previous research was which conducted by Vashistha et al. [12]. The treated WCP is divided into two groups, burned and milled WCP (BMWCP) and milled WCP (MWCP). In Fig. 2(a), the TGA analysis of the treated WCP is presented. Notably, the highest weight loss for the BMWCP was observed at the temperature range of 600°C to 700°C, which is related to the decomposition of the residual calcium carbonate after 2 hours of calcination. In contrast, MWCP and the as-received WCP demonstrated three distinct weight loss peaks. The weight loss at the temperature range of 50°C to 200°C is associated with the loss of the free water and chemically bound water of the hydrated cement phase. Further decomposition was observed between 320°C to 490°C related to the removal of organic impurities particularly asphalt which was present in raw material [30,31]. Finally, the third peak is due to the decomposition of the calcium carbonate from 600°C to 700°C [12]. Hence, in the preparation of BMWCP as a binding material, a moderate temperature of 650°C for 2 hours was chosen for thermal treatment to generate reactive phases and decrease carbon dioxide emissions. The aim of the calcination of the WCP was to eliminate asphalt and dehydrate the cementitious phases, resulting in a burned WCP material. Subsequently, the burned WCP material was cooled at room temperature to avoid the generation

Table 1
XRF analysis of WCP and Metakaolin.

Oxide composition	Weight (%)									
	CaO	Al_2O_3	SiO_2	MgO	TiO_2	SO_3	Fe_2O_3	K_2O	Others	LOI
WCP	29.1	5.6	25.2	1.7	1.2	1.8	13.2	2.7	2.5	15
BMWCP	16.3	12.9	52.1	2.5	0.4	1.3	3.8	3.3	1.8	5.6
MK	0.5	43.3	50.4	0.2	2.3	0.1	2.8	-	0.5	-

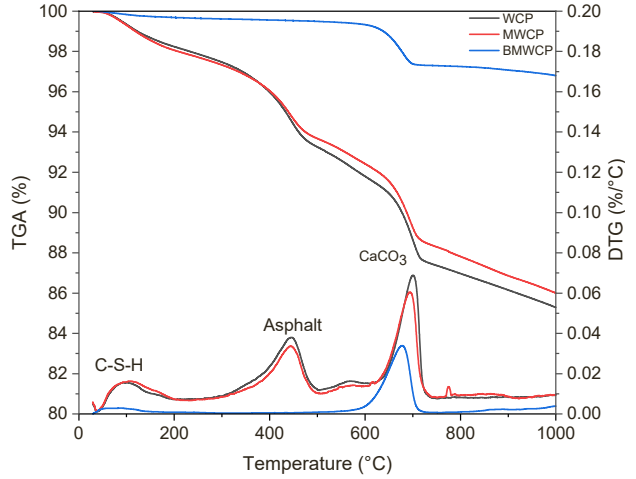

(a)

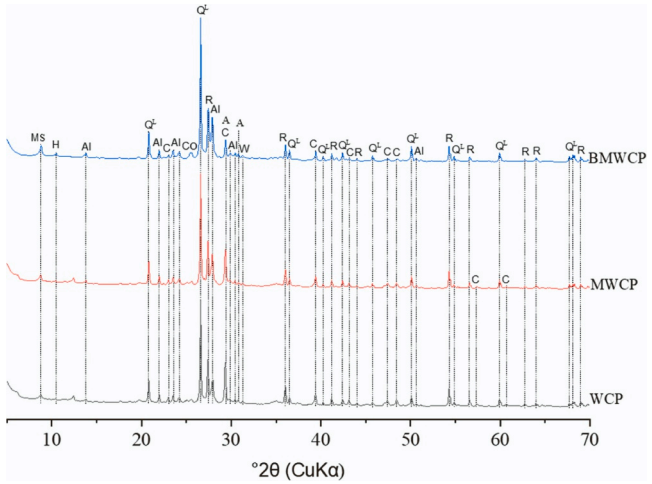

(b)

Fig. 2. (a) TGA curve comparison of WCP and Treated WCP, (b) The mineralogical composition of raw WCP, Burned, and Milled WCP, magnesium silicate (MS), alite (A), hemicarbonate (H), albite (Al), wollastonite (W), quartz-Low (QL), coesite (CO), calcite (C), rutile (R).

of more phases. Once the necessary cooling was attained, milling was undergone by the material. For the milling process, a diameter range between 30 mm and 5 mm of mixed steel balls was used for two hours. Furthermore, MWCP was produced by employing only a similar milling process of WCP, as BMWCP production, to increase the fineness of the WCP to the required range. Subsequently, the XRD analysis of the WCP, MWCP, and BMWCP are presented in Fig. 2(b). The primary phases were magnesium silicate, hemicarbonate, albite, wollastonite, quartz-Low, coesite, calcite, rutile, alite. Furthermore, the physical properties of the materials are summarized in Table 2. Different proportions of MWCP and BMWCP were prepared with the addition of metakaolin and alkali, solution was subsequently utilized for sample preparation.

Table 2
Physical properties of the treated WCP.

Description	Specific gravity	Particle size distribution (μm)		
		d_{10}	d_{50}	d_{90}
WCP	2.03	174.5	469	724.3
MWCP	2.14	1.7	8.9	60.4
BMWCP	2.30	1.8	8.9	40.6

2.3. Chapelle test

The Chapelle test serves as a crucial assessment tool for determining the consumption of lime by the reactive silica in materials [32]. It was performed to check if the reactive silica is present in the WCP, MWCP, and BMWCP. The presence of reactive silica in any sample will provide a base to utilize it as a precursor in alkali-activated binder systems.

The principle involves lime's reaction with the reactive silica, measuring free lime consumption in milligrams (mg) of CaO per gram of WCP. Lime utilization is assessed based on a specific lime-to-WCP mass ratio of 2:1 [32,33]. The testing procedure is presented in Fig. 3. The lime consumption is calculated using Formula (1) provided below. This method enables quantification of lime utilization by WCP, aiding in assessing its suitability as a precursor [32]:

$$mg\ CaO\ per\ gram\ of\ material = \frac{28 \times (v_2 X m_3 - v_1) \times F_c \times 2 \times 2}{m_1 \times \quad m_2 \times \quad m_3} \qquad (1)$$

Where:

v_2 = Consumption of 0.1 M HCL by the blank solution millilitres
m_1 = Weight of WCP in grams
v_1 = Consumption of 0.1 M HCL by sample solution in millilitres
m_2 = Weight of WCP and CaO in grams
F_c = Correction factor of standard solution HCl 0.1 M
m_3 = Weight of CaO in blank test in grams

2.4. Binder and specimen preparation

The alkali-activated binder was produced with an alkali activator ($NaSiO_3$ + NaOH) to binder (MK + (B)MWCP) ratio of 0.5. A commercial Sodium silicate solution, comprising 62 % H_2O, 10 % NaO_2, and 28 % SiO_2 with a specific gravity of 2.3 and a SiO_2/Na_2O molar ratio of 2.9, was employed. Additionally, Sodium hydroxide with 98 % purity was used to prepare a solution with a molarity of 14 and 12 M. In the case of the pure metakaolin based samples, the S/A molar ratios were 2.28 and 2.31 for the reference samples, while these ratios vary with the incorporation of the MWCP and BMWCP. The solution was mixed for 5 minutes with the metakaolin and WCP precursors. The water-to-solid (w/s) ratio varies with respect to the alkali ratios. Both BMWCP and MWCP were incorporated in the mixture separately by replacing metakaolin at a range from 10 % to 80 % of the total precursor weight, with an increment of 10 %.

Table 3 provides a summary of mix proportions, specifying specimen names by use of MWCP and BMWCP. Post-mixing, the alkali-activated paste was cast in 50 × 50 × 50 mm cubic molds and demoulded after one day. Subsequently, the specimens were cured under sealed conditions at 60 °C for 72 hours and conducted compressive strength tests of

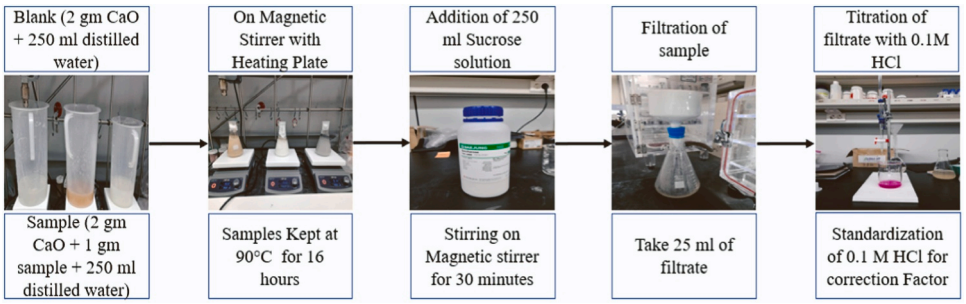

Fig. 3. Flow chart representing the modified Chapelle test [28].

Table 3
Mix proportion of the samples.

Description	SSS/NH	M	W/S	Ms	kg/m^3				
					MK	MWCP	NH	SSS	Water
1.5Ref	1.5	14.0	0.41	0.8	1067.0	0.0	213.0	318.0	379.0
1.5MW10					960.0	107.0			
1.5MW20					853.0	213.0			
1.5MW30					747.0	320.0			
1.5MW40					640.0	427.0			
1.5MW50					533.0	533.0			
1.5MW60					427.0	640.0			
1.5MW70					320.0	747.0			
1.5MW80					213.0	853.0			
2Ref	2.0	12.0	0.43	1.0	1067.0	0.0	178.0	356.0	3370.0
2MW10					960.0	107.0			
2MW20					853.0	213.0			
2MW30					747.0	320.0			
2MW40					640.0	427.0			
2MW50					533.0	533.0			
2MW60					427.0	640.0			
2MW70					320.0	747.0			
2MW80					213.0	853.0			
Description	SSS/NH	M	W/S	Ms	kg/m^3				
					MK	BMWCP	NH	SSS	Water
1.5Ref	1.5	14.0	0.41	0.8	1067.0	0.0	213.0	318.0	379.0
1.5BMW10					960.0	107.0			
1.5BMW20					853.0	213.0			
1.5BMW30					747.0	320.0			
1.5BMW40					640.0	427.0			
1.5BMW50					533.0	533.0			
1.5BMW60					427.0	640.0			
1.5BMW70					320.0	747.0			
1.5BMW80					213.0	853.0			
2Ref	2.0	12.0	0.43	1.0	1067.0	0.0	178.0	356.0	370.0
2BMW10					960.0	107.0			
2BMW20					853.0	213.0			
2BMW30					747.0	320.0			
2BMW40					640.0	427.0			
2BMW50					533.0	533.0			
2BMW60					427.0	640.0			
2BMW70					320.0	747.0			
2BMW80					213.0	853.0			

SSS: sodium Silicate Solution, MK: Metakaolin, M; Molarity, NH: Sodium Hydroxide, SS: Sodium Silicate, Ms (Modulus)= SiO_2/Na_2O molar ratio, W/S = water-to-solid ratio

the 3 days oven cured samples. Subsequently, part of the crushed specimens were broken into small pieces for the MIP testing and pulverized with a mortar and pestle for the TGA and XRD studies. To remove the free water with isopropanol, the ground or fractured specimen was immersed in isopropanol (10 mL/g) for one hour. Following the suspension's filtering ether, the samples were vacuum-dried, then dried again for ten minutes at 40 °C in an oven, and stored in a desiccator until testing [34].

2.5. Characterization of alkali-activated mixture paste

Distinct alkali-activated binder paste mixtures underwent comprehensive characterization through various analytical methods. Isothermal calorimetry, utilizing the ICal 2000 H model from TA Instruments USA, was employed in accordance with ASTM C1702 [35]. The whole procedure was conducted within around 1.5 minutes. The hydration kinetic analysis continued for 7 days at the 25°C temperature of the instrument. As mentioned in Section 2.4, after mixing and casting the samples in the mold, the samples were left at room temperature of 25

°C for the first 24 hours. Afterward, the hardened samples were demolded and cured in an oven for another 3 days at 60 °C. Considering these two conditions, it was decided to conduct the test at 25°C to track the heat release over 7 day period by maintaining the first 24 hours condition of the samples. Similar working conditions were employed in the previous studies [36,37].

XRF served as a non-destructive analytical tool to ascertain the elemental composition of WCP. XRD was performed to analyse mineralogical characteristics of the WCP, and hydrated samples by using Bruker D8 Advance instrument at room temperature with a scanning rate of 3°/min, and X'Pert High Score Plus and PDXL software facilitated crystalline phase identification. Moreover, TG/DTG analysis was conducted by using TGA SII Seiko Instrument EXSTAR. TGA was carried out in a nitrogen atmosphere at a rate of 10 °C/min with a temperature range of 30–1000 °C. Spectroscopic study employed with the use of 670/620 model Varian instrument for Fourier Transform Infrared (FT-IR). The samples were scanned within the range between 400 and 4000 cm^{-1} with 4–32 scans per spectrum. MIP analysis involved fracturing samples, collecting pieces smaller than 20 mm, and employing the solvent exchange method for drying [34]. The MIP test, conducted with the AutoPore VI 9620 instrument from Micromeritics Instrument Corp, was performed with a sample size below 0.5 cm. The pore sizes were measured up to 360 μm by applying pressures ranging from 0.2 to 413.7 MPa.

2.6. Life cycle analysis (LCA)

To assess the carbon footprint of the manufactured binder, it is essential to consider the materials involved (metakaolin, alkali solution, and activated WCP) and their respective production processes. The binder formulation is already detailed in the experimental procedures.

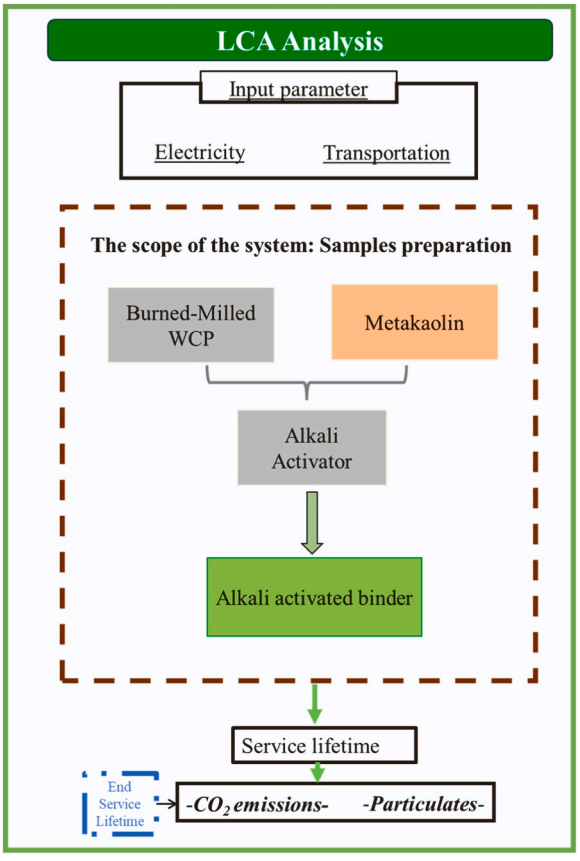

Fig. 4. Alkali-activated WCP based cementless binder manufacturing system boundary.

Fig. 4 outlines the system boundary, with a primary focus on comparing the WCP-based alkali-activated binders comparing with the metakaolin-based geopolymer and OPC.

Simapro 9.3.0.3 software and IMPACT World + Midpoint V1.01 method were employed to evaluate the impact of the alkali-activated binder on the environment. The dataset for cement (type 1) production included activities from cradle to grave, covering all upstream activities leading to final production in the mill, and was globally modelled for cement production. For electricity consumption during the WCP activation process, the Korean scenario was utilized, and carbon emissions were calculated based on experimental analyses.

In this study, the alkali-activated WCP cementless binder production phase was considered in the system boundary, disregarding the influence of the developed binder on the environment in its lifespan. Therefore, transportation, material involvement, and energy were considered into account in the production process. The LCA compares the environmental impacts of WCP-based binder with, geopolymer and OPC. Input data for grinding and thermal treatment come from electricity usage by the milling and furnace. Electricity consumption during WCP activation is based on 2018 IEA statistics. Output data, including organic compound emissions from WCP thermal treatment, are sourced from the EcoInvent database [38].

3. Results and discussion

3.1. Chapelle test analysis

The consumption of lime can serve as an indicator of the reactivity of the material [39]. Consequently, the WCP, MWCP, and BMWCP were subjected to testing to investigate the pozzolanic reactivity improvement of the material pre and post treatment by determining the amount of CaO consumed, as depicted in Table 4. Each material underwent testing three times, and the provided findings represents the average of the repeated tests. The tests demonstrate minimal variance in the CaO consumed by the treated and untreated WCP, indicating the consistency of the material.

Subjecting both milling and calcination on WCP enhanced the amount of the reactive silica present in the material which led consumption of more CaO. Therefore, this suggests that MWCP consumed more CaO compared to WCP, while BMWCP exhibited the highest CaO consumption. Hence, the thermal and mechanical treatment of WCP proves advantageous in enhancing reactivity of WCP as a precursor with metakaolin to produce an alkali-activated binder.

3.2. Compressive strength of alkali-activated mixtures

Fig. 5 represents the compressive strength development of different blends of alkali-activated mixtures. The research explores how the compressive strength of alkali-activated mixtures is influenced by factors such as the composition and concentration of the alkaline solution, as well as the quality and quantity of WCP powder incorporated. Fig. 5 also illustrates the impact of the SSS/NH ratio on the compressive strength at various MWCP and BMWCP application proportions. Elevating the SSS/NH ratio from 1.5 to 2 is correlated with an increase in compressive strength with more than 30 % application of BMWCP. This rise in strength is attributed to delayed setting and an augmented SiO_2/Na_2O ratio [36,40,41]. The delayed setting phenomenon is linked to the

Table 4
The consumption of Calcium by WCP in terms of CaO (mg/g).

Description	CaO Consumption		
	Minimum	Maximum	Average
WCP	897.1	943	920
MWCP	1028.3	1036.5	1032.4
BMWCP	1125.2	1155.7	1140.4

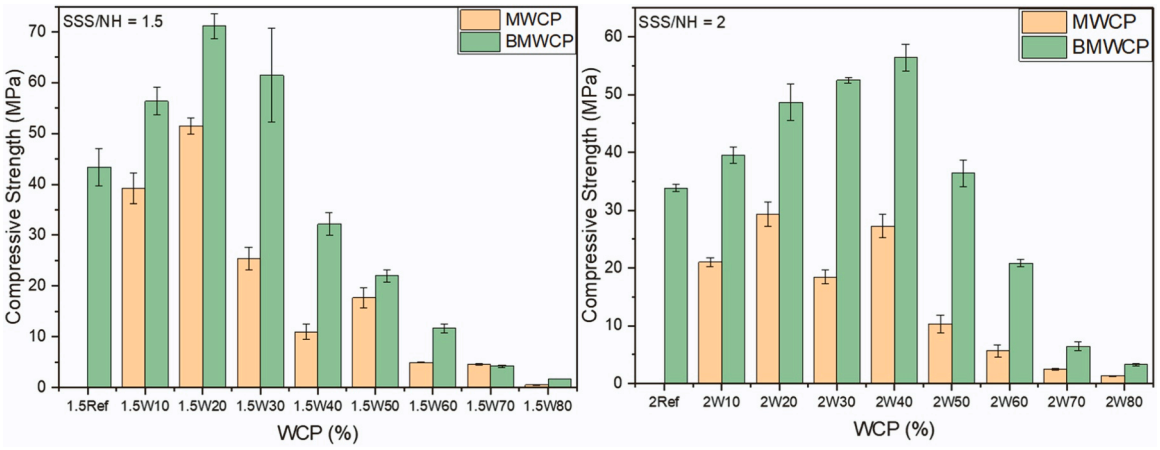

Fig. 5. Compressive strength of mixtures with various treated WCP.

addition of SSS in both calcium (Ca)-augmented geopolymer systems and metakaolin-based systems since the increment of the Si/Al molar ratio leads to the increase in setting time [42]. It was also observed in a study by Pacheco-Torgal et al. [43] that flash setting in an alkali system derived from tungsten mine tailings at high NaOH concentrations when $Ca(OH)_2$ was introduced. This challenge was successfully addressed by enhancing the SSS/NH ratio. The rationale behind this lies in the high alkalinity and rapid dissolution of Ca-silicate minerals such as alite, leading to the precipitation of $Ca(OH)_2$ on particle surfaces [36,40]. This precipitation impedes further dissolution of Si and Al. In other words, the addition of soluble silicates means increasing the SiO_2/Na_2O molar ratio, which leads to the reduction of the dissolution of the Si and Al. Another contributing factor to the positive influence of the SSS/NH ratio on compressive strength is the presence of available soluble silicates. In the alkali activation process, the initial step involves the dissolution and hydrolysis of silica and alumina from the solid aluminosilicate source. Hydrolysis of these minerals results in the formation of Si-OH and Al-OH bonds, followed by condensation [44]. This phenomena of silicates and aluminates phases condensation were predominantly visible in the mixtures with BMWCP. As another factor responsible for more compressive strength in the case of 2BMW40 than 1.5BMW40 is the presence of more soluble silicate in the alkaline solution, the hydrolysis process is accelerated, facilitating a faster geopolymerization process. This intricate interplay of factors highlights the nuanced relationship between the SSS/NH ratio and the availability of soluble silicates, all contributing to the enhanced strength observed in the 2BMW40 blend.

Other than the presence of more silicates in the BMWCP mixture, the presence of reactive calcium also plays a significant role in the development of more compressive strength [12]. The enhanced performance observed with BMWCP can be attributed primarily to the contribution of calcium (Ca) and silicon (Si) in facilitating the development of C-S-H and geopolymeric gels [45,46]. The introduction of Ca into the geopolymeric system plays a dual role: it not only accelerates the dissolution process but also promotes hardening by providing additional nucleation sites, as highlighted by studies [47,48]. However, it's important to highlight that the beneficial impact of Ca on the geopolymeric system is subject to a certain threshold, as observed by various researchers [49,50]. In the current investigation, the positive effect of BMWCP is capped at a 50 % addition of WCP. Beyond this point, mixtures developed less compressive strength than reference mixtures. There are two possible scenarios, which can significantly affect the performance of the samples. First is the dilution effect at which the geopolymeric gels formation significantly reduces with the increase of the BMWCP. This is because the metakaolin is amorphous and more reactive than BMWCP in an alkali solution environment. Losing the dominance of the metakaolin in the matrix means the generation of less geopolymeric gel, negatively affecting the mechanical performance of the samples [51]. Secondly, the crystalline phases in BMWCP, anorthite, wollastonite, and alite, undergoes a dissolution in the alkali solution. The relation calcium ion in a high pH environment leads to the early precipitation of calcium hydroxide. Consequently, the alkalinity in the matrix reduces which means hindering the formation of geopolymeric gels [52–54]. Understanding these limitations is crucial in optimizing the formulation of geopolymeric systems for improved strength and performance.

3.3. Characterization of alkali-activated mixtures

3.3.1. XRD analysis

To understand the changes in hydration phases, 20, 40, 60, and 80 percent replacement of both MWCP and BMWCP were chosen and compared with the Ref samples, since they demonstrated a notable difference in the compressive strength. The XRD analysis was performed after 3 days of oven curing to determine the effect of MWCP and BMWCP on the alkali-activated mixtures. Illustrated in Figs. 6 and 7 are the diffraction patterns corresponding to various paste samples, revealing distinctive peaks associated with specific phases. The diffraction patterns highlight the presence of peaks characteristic of quartz, calcite, enstatite, alite, albite, faujasite, and portlandite in BMWCP and MWCP incorporated samples. On the other hand, anatase, muscovite, and kaolin were detected in the reference samples regardless of the alkali ratios. These patterns serve as a visual representation of the crystalline phases identified within the respective paste samples, aiding in the characterization, and understanding of the material composition based on established diffraction standards. As can be seen in Figs. 6 and 7, samples with BMWCP and MWCP, albite, and enstatite, were detected. These minerals, which are from the aggregate, demonstrate insignificant change. However, the faujasite peak initially increased with the increase of BMWCP and MWCP and then the peak significantly reduced. The formation of this phase is associated with the reduction of the Si/Al molar ratio as the replacement of the metakaolin since BMWCP and MWCP both have less amorphous silica. This leads to the formation of the faujasite, however, due to the higher replacement of the metakaolin, the formation of this phase declined.

Figs. 6(a) and 7(a) represent the XRD spectrum of the mixtures with SSS/NH ratios of 1.5 and 2, respectively. In the comparison of the mixtures, majorly two trends were observed with the crystalline peaks. Firstly, the intensity of the calcite peak decreased in the case of the mixtures with BMWCP. The trend of calcite peak intensity reduction is attributed to the presence of the reactive calcium inform of portlandite which contributes to the hydration process [55]. However, mixture 1.5BMW80 resulted in a predominant calcite peak due to the presence of residual calcite during the thermal modification of the MWCP to get the BMWCP [12]. The second trend in the peaks was observed with the quartz peaks which have more intensity in the mixtures with MWCP. As

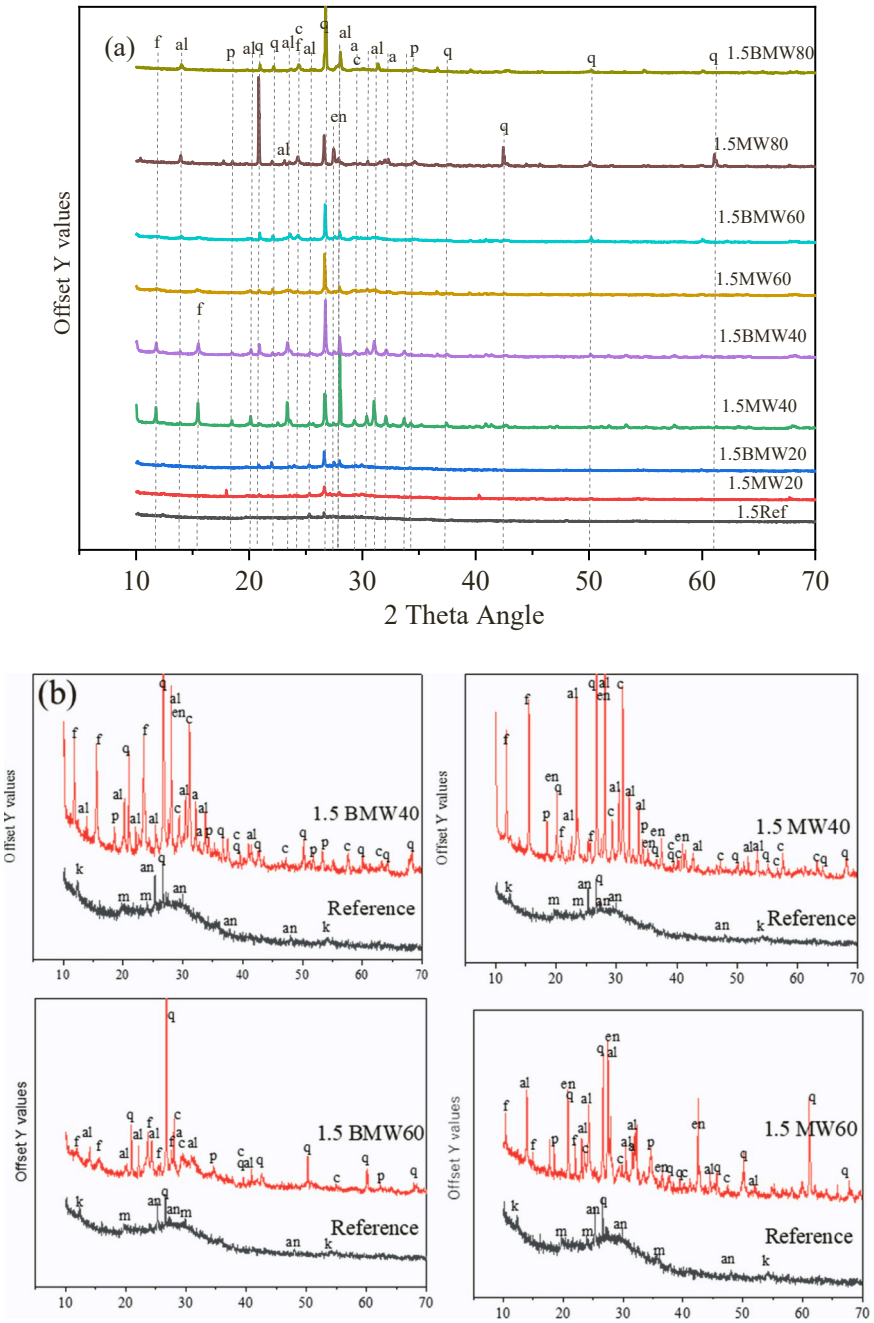

Fig. 6. (a) XRD spectrum of alkali-activated binder with SSS/NH =1.5 pastes after 3 days of oven curing, (b) Comparison of reference with 1.5 SSS/NH to different q: quartz, c: calcite, en: enstate, a: alite, an: anatase, m: muscovite, al: albite, f: faujasite, k: kaolin, p: portlandite.

discussed in Section 3.1, BMWCP has more reactive silica than MWCP, this reactive silica participates in the hydration process and geo-polymerization reaction which consumes silica in the case of BMWCP.

Figs. 6(b) and 7(b) represent the comparison of the MWCP and BMWCP mixtures with the reference mixtures with individual spectrum. This kind of depiction of XRD spectrums is helpful in understanding the hump formation to check the presence of amorphous phases. In Figs. 6 (b) and 7(b), this broad hump was observed in both the reference and BMWCP samples while the broad hump was not observed in the MWCP based mixtures. This amorphous hump, spanning approximately 20° to 40°, relates to the geopolymeric gel and the characteristics of the raw metakaolin. On comparison between the BMWCP mixtures of an SSS/NH ratio of 1.5 and an SSS/NH ratio of 2, the broad hump was more dominant in the case of an SSS/NH ratio of 2. It was also observed that hump formation was most predominant in the case of mixture 2BMW40 among all the mixtures. This outcome attributes the formation of most geopolymeric reactions and the formation of most geopolymeric gel and C-A-S-H gel in the case of mixture 2BMW40. This argument for XRD analysis is in line with the compressive strength development for the different mixtures.

Notably, in the mixture 2BMW40, a semi-crystalline phase emerges, evident in humps centered at approximately 30° and 40°. This phenomenon is attributed to the generation of low calcium C-S-H gel, as also observed by Saeed et al. [51] in a concrete waste with a fly ash geopolymer system. The development of C-S-H gel with the coexistence of geopolymeric gels has been observed by several researchers [56–60]; for instance, Mackenzie et al. [61] reported that added calcium was integrated into the geopolymer network. In the current study, based on

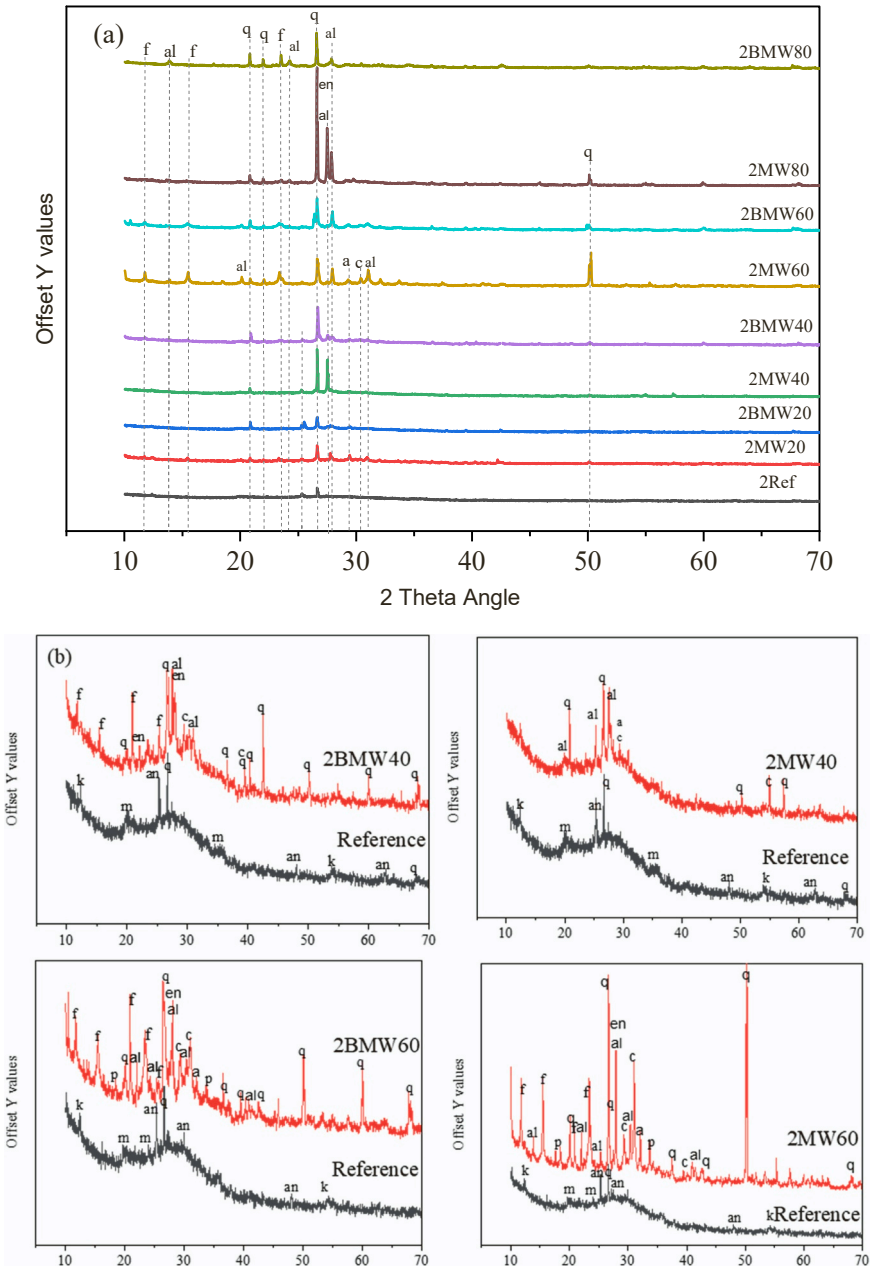

Fig. 7. (a) XRD spectrum of alkali-activated binder with SSS/NH =2 pastes after 3 days of oven curing, (b) Comparison of reference with 2 SSS/NH to different mixtures q: quartz, c: calcite, en: enstate, a: alite, an: anatase, m: muscovite, al: albite, f: faujasite, k: kaolin, p: portlandite.

compressive strength and mineralogical analysis of the various mixtures, it is suggested that BMWCP as a calcium and silica source can be simultaneously incorporated into the geopolymer network while contributing to the formation of low calcium C-S-H gel. Further study is needed to confirm the type of C-S-H gel formed and its properties in this system. However, due to the high alkalinity, the predominant product of the reaction is the geopolymer gel [62].

3.3.2. TG and DTG analysis

To further understand the hydration products developed in the samples, TG/DTG analysis was performed. The results of the 40 % and 60 % replacement of the BMWCP and MWCP with different SSS/NH ratios compared with the reference samples are illustrated in Fig. 8(a) and (b). The total weight loss of the samples with the SSS/NH ratio of 1.5 demonstrated higher weight loss than those samples with the SSS/NH ratio of 2. However, the reference samples of both ratios showed the opposite, even though the difference is relatively small. The amount of weight loss of the BMWCP based samples demonstrated almost identical trends regardless of the alkali ratio, while the MWCP demonstrated three separate peaks in the SSS/NH ratio of 1.5 and 2 throughout 1000°C.

Firstly, the weight loss of the temperature ranging from 50°C to 250°C relates to the loss of the water in the geopolymeric gel structure and the decomposition of the C-A-S-H or C-S-H gel due to chemically bound water [54,63]. Comparing the BMWCP with the reference samples in both cases of alkali ratios, the weight loss peak corresponding to this temperature range initially increased with the 40 % BMWCP incorporation as a metakaolin replacement. However, replacing 60 % of metakaolin with BMWCP demonstrated a lower weight loss, which might be attributed to the reduction of the geopolymeric gel domination in the matrix due to the dilution effect. Considering the SSS/NH ratios, 1.5BMW40 exhibited higher weight loss compared to the 2BMW40. However, the case of the 1.5BMW60 demonstrated the opposite, which

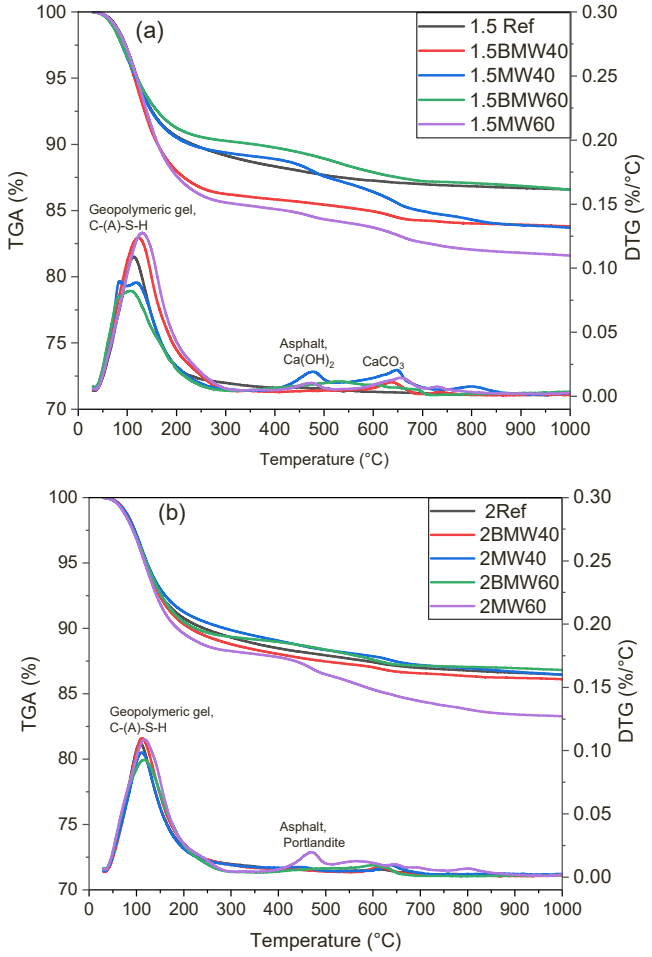

Fig. 8. TGA and DTG results (a) SSS/NH ratio of 1.5. (b) SSS/NH ratio of 2.

is the lowest weight loss among the samples regardless of the alkali ratios. Therefore, it can be understood that the lower SSS/NH ratio favored the formation of more geopolymeric gel with the samples of a higher amount of metakaolin than the higher content of BMWCP in the matrix due to the high concentration of the alkaline environment [45]. Nevertheless, a higher SSS/NH ratio promotes the coexistence and the contribution of the C-S-H gel with geopolymeric gel due to the available reactive calcium and soluble silica in the matrix [45,64].

On the other hand, In the case of MWCP, initially, a decline was observed in the first peak in the samples with 40 % of MWCP compared with the reference samples regardless of the alkali ratio. This reduction signifies a decrease in the extent of geopolymer formation. Subsequently, the peak intensifies with the incremental inclusion of MWCP60, particularly evident in SSS/NH ratios of 1.5 and 2. This augmentation can be attributed to the decomposition of hydrated cement and the presence of impurities within the raw materials [12,65]. As can be seen in Figs. 8, 1.5MW40 demonstrated higher weight loss than 2MW40. However, when MWCP content increased up to 60 %, the opposite phenomenon of weight loss was observed in the temperature range of 50°C to 250°C. In both cases of alkali ratios, the MWCP was further decomposed at the temperature range from 420°C to 490°C and can be related to the combustion of the asphalt present in the raw material and the decomposition of portlandite [34,66]. Finally, all samples except the reference samples experience weight loss at the temperature from 580°C to 680°C, which can be related to calcite [34,67]. Notably, it is not possible to reach a conclusion based on the weight loss analysis since almost all samples demonstrated identical weight loss.

3.3.3. Hydration kinetics of mixtures

Fig. 9 illustrates normalized heat flow and normalized heat for 40 % WCP and reference mixtures. The normalized heat is proportional to the hydration degree, while the normalized heat flow can be associated with the rate of hydration for the samples. Upon the amalgamation of the activator with the precursor, an exothermic peak promptly manifests, indicative of the wetting and dissolution of the solid material [68]. This distinct peak shares similarities with the initial phase of cement hydration, akin to the pre-induction period, despite potential variations in the underlying physicochemical reactions [69].

Following the initial dissolution peak, there ensues a brief dormant phase succeeded by a subsequent expansive exothermic peak. After the initial dissolution, the concentrations of dissolved ionic species attain a critical threshold, signalling the initiation of subsequent reactions. This dormant interval, analogous to the induction period in cement hydration, is presumed to represent the duration required for concentration elevation [68]. The second peak is predominantly attributed to the exothermic processes of polymerization and condensation in geopolymer gels [69]. Illustrated in Fig. 9(a), the intensity of the second peak was highest in the case of mixture 2 reference. However, this peak was the longest in the case of the 2BMW40 mixture, which is attributed to the polymerization and formation of the geopolymer gels for a longer time.

The geopolymerization extent of raw materials can be characterized by heat evolution: the more reaction heat the system releases, the higher the extent of geopolymerization it obtains [69]. Fig. 9(b) and (c) represent the cumulative heat evolved by the mixture. The application of MWCP and BMWCP in the case of the mixture with SSS/NH 1.5 resulted in a decrease in the cumulative heat of hydration in comparison to the reference mixture. The 1.5 reference mixture evolved 118.3 J/g, while 1.5 MW40 and 1.5 BMW40 evolved 74.1 J/g and 92.7 J/g of heat, respectively. However, in the case of SSS/NH 2, mixture 2BMW40 evolved the maximum heat of hydration among all the mixtures with 147.6 J/g, which was higher than the reference sample. This outcome of heat evolution in the case of mixture 2BMW40 is attributed to the development of most geopolymer hydration products among all the mixtures, which is also associated with the compressive strength results and XRD analysis results.

3.3.4. FTIR analysis

In order to avoid the flash setting caused by a high concentration of sodium hydroxide in the calcium precursor material and reduce the amount of the WCP consumption, as elucidated in Section 3.2, Fig. 10 represents the FTIR analysis of SSS/NH ratio of 2, which depicts the structural transformations. This analysis involves a comparison of the reference sample with the 2BMW40 and 2BMW60 following three days of oven curing. The spectra offer insights into the alterations occurring within the mixtures. Specifically, in Fig. 10(a) and (b) the peak centered around 970 cm^{-1} of 2Ref corresponds to the vibration of O-Si-O bonds, signifying the binding vibration of O-Si-O bands and the stretching of SiQ_n units (where n = 4, 3, 2, 1, and 0) [70–72]. This characteristic feature is ascribed to the stretching vibrations of SiO_4 tetrahedra in aluminosilicates of the alkali-activated mixtures, specifically the Si-O stretching vibrations [73–75]. The center of this peak shifts towards a lower wavelength with the incorporation of both BMWCP and MWCP compared to the reference sample. This shift from 970 cm^{-1} to 945 cm^{-1} could be attributed to the reduction of the degree of polymerization, which possibly occurred due to the substation of the Al and Ca with the silicate bond developed as a result of the reaction between BMWCP/ MWCP and alkali solution [24,46,72,76,77]. However, comparing the samples with BMWCP and MWCP, 2BMW40 demonstrated a higher degree of geopolymerization than the mixture 2MW40, 2MW60, and 2BMW60. The more pronounced shift observed in the 2BMW40 suggests a heightened degree of alkali activation within the systems with calcium.

The presence of calcite was detected through the observation of an

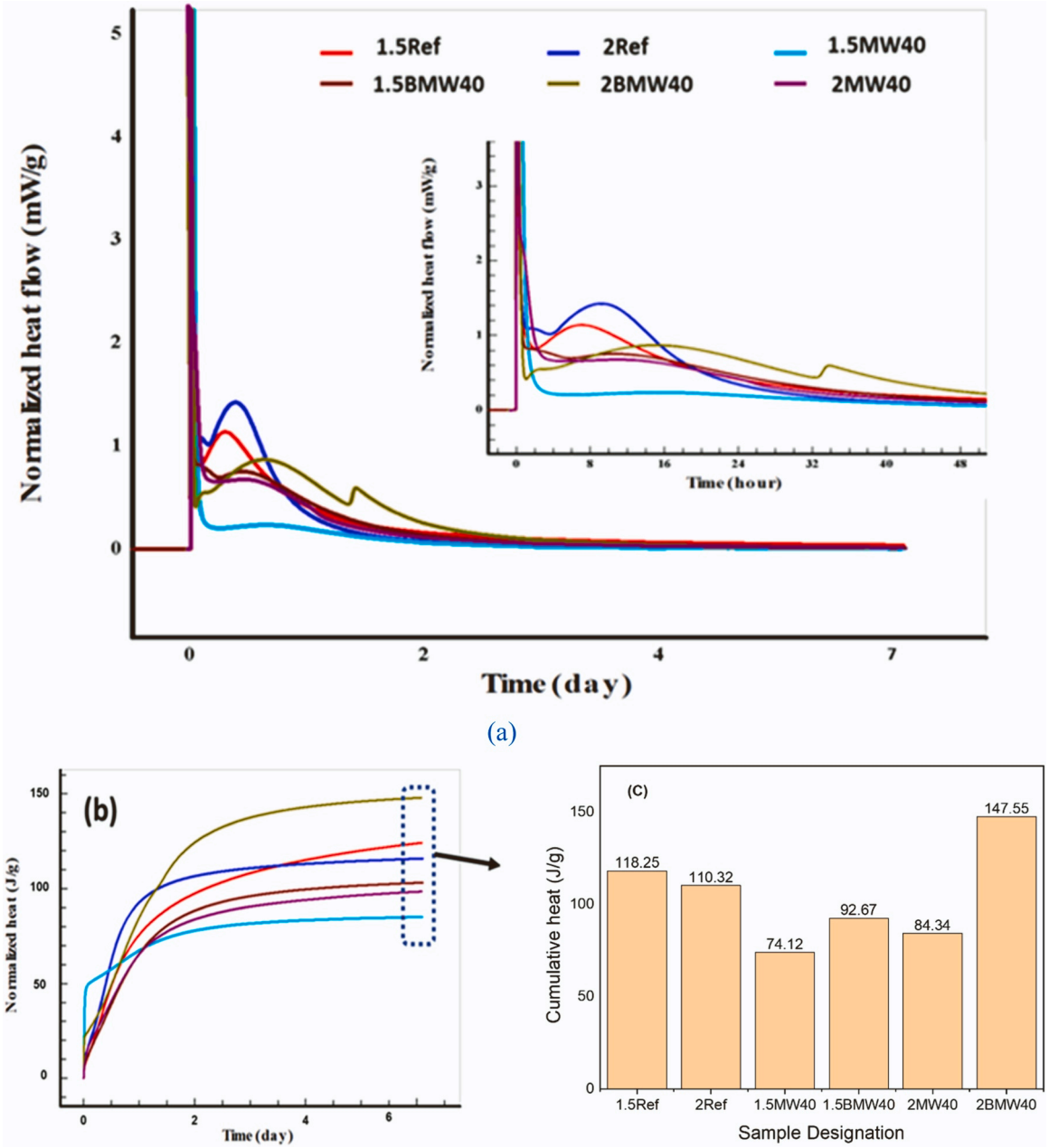

Fig. 9. (a) Normalized heat flow, (b) Normalized heat, and (c) Cumulative heat of hydration at 7 days for different mixture paste.

absorption hump spanning the spectral range from approximately 1409 cm^{-1} to 842 cm^{-1}. These spectral bands are indicative of the out-of-plane bending vibration (v4) and the asymmetrical stretching vibration (v3) associated with the (C-O) bond characteristic of calcite [10, 78]. Fig. 10 (a) and (c) illustrate the (C-O) stretching, which is more pronounced in 2MW60 and 2BMW60 while least in 2Ref and 2BMW40 mixtures. Importantly, 2BMW60 exhibits a more intensified band than other mixtures, signifying a higher degree of carbonation. This intensified carbonation may explain the decline in compressive strength due to the formation of calcite, which is also evident from the XRD spectrum of the mixture 2BMW60 in Fig. 10(a). A noteworthy aspect of the study involved the identification of the O-H group's stretching and deformation modes, observed at 1600 cm^{-1}. The FTIR spectra analyzed across different mixtures, excluding the 2Ref, affirm the existence of C-S-H gel and calcite [12]. This phenomenon corresponds harmoniously with both the strength analysis and the mineralogical scrutiny of the mixture, thereby supporting our full comprehension of the observed results.

3.3.5. *Mercury Intrusion Porosimeter analysis (MIP)*

The assessment of the mechanical properties of binder pastes critically relies on the distribution of pore sizes and overall porosity [79–81], especially considering the properties of the interfacial zone between geopolymer gel and WCP. In Fig. 11, the effect of MWCP and BMWCP on the microstructure development of 1.5Ref, 2Ref, 1.5MW40, 1.5MW60, 1.5BMW40, 1.5BMW60, 2MW40, 2MW60, 2BMW40 and 2BMW60 are illustrated. The average pore size in the samples spans between 7.7 and 72.7 nm. Notably, the mixtures with BMWCP exhibited the smallest pore diameter among all paste samples. For a quantitative assessment, Table 5 summarizes the average pore size and total porosity. The WCP state has a discernible influence on the paste porosity. In contrast to reference mixtures, the porosity increases for MWCP based mixtures, while it decreases for BMWP based mixtures. As highlighted by Aredes et al. [82] and Deventer et al. [83], examining the porosity characteristics of geopolymer samples involves considering the alkaline hydrolysis-induced dissolution of solid aluminosilicate, a process that

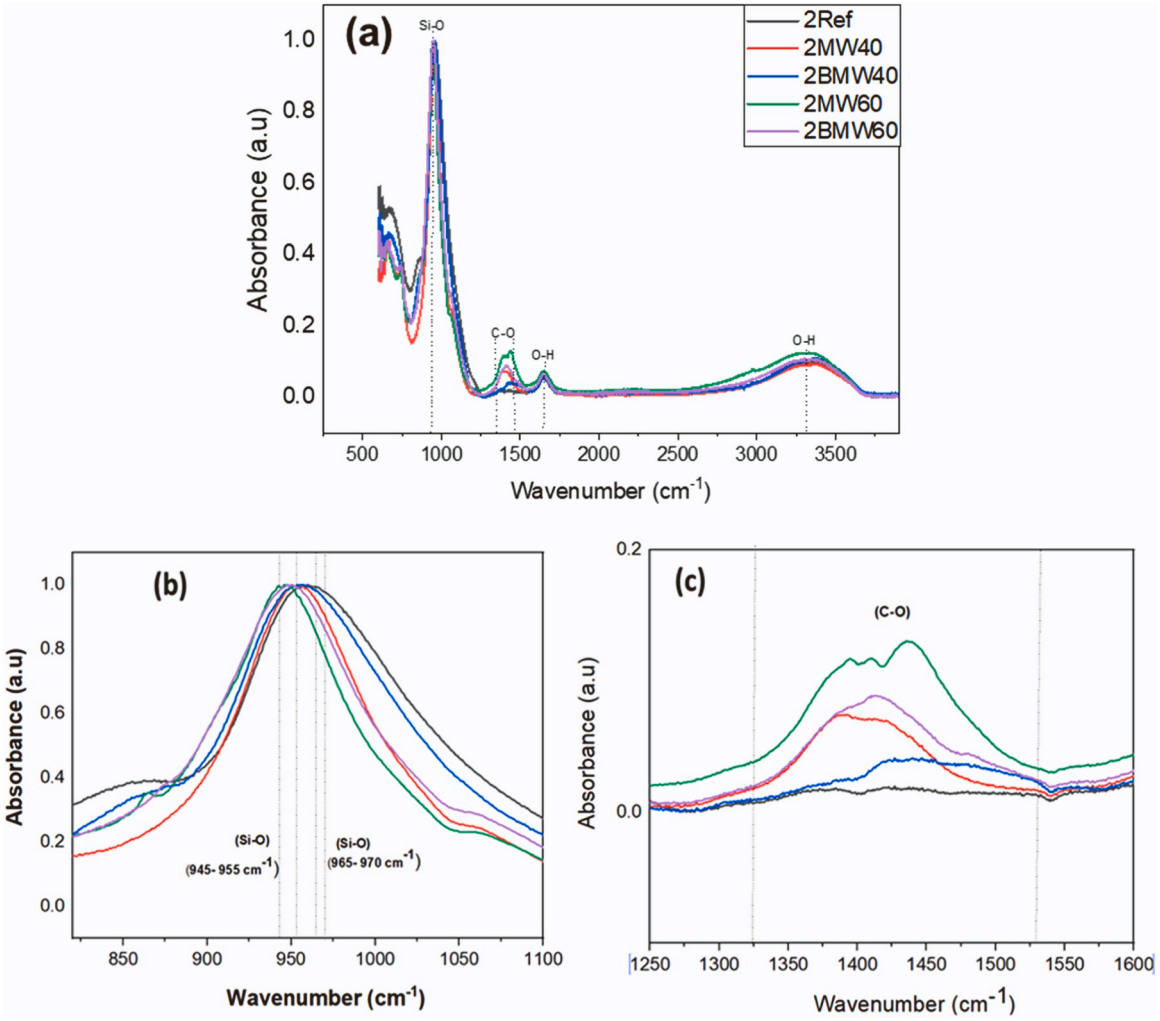

Fig. 10. (a) FTIR spectra of mixtures (b) at 955 and 965 cm^{-1} (c) 1409 cm^{-1}.

consumes water and generates a supersaturated solution of aluminate and silicate species, ultimately leading to gel formation. Following gelation, the system undergoes reorganization, releasing water molecules that were initially consumed during the dissolution process. These water molecules effectively occupy the solid gel structure, and the voids left after the drying phase define the porosity structure of the samples. In context to this mechanism, BMWCP based samples should have the highest total porosity, however, in calcium based alkali-activated binder system another mechanism also worked as suggested in the studies by Zhao et al. [84], Shao et al. [85], and O'Farrell et al. [86], due to pozzolanic reaction, more hydrated phases were produced by the reaction of the portlandite hydration and supplementary cementitious materials (SCM). Consequently, the reduction of the porosity was observed due to the occupation of the C-S-H gel in the pore space.

4. LCA analysis

In Fig. 12 visually depicts the flow chart outcomes for four distinct binder mixtures: OPC, 2 reference, and 2BMW40. At all levels, incorporating activated WCP in lieu of metakaolin yielded a notable reduction in environmental impact. According to the previous study, which was conducted by Vashistha et al. [12], per ton of OPC production released in 878 kg of CO_2. The calculation also considers CO2 emissions arising from both the transportation of cement from the plant to the market, which involves heavy transport, and the subsequent transportation from the market to the laboratory, which typically involves lighter transport. [87]. In comparison, the metakaolin-based geopolymer binder, specifically the 2-reference sample, exhibited a 47.3 % decrease in carbon emissions compared to OPC. Furthermore, the incorporation of 40 % BMWCP with metakaolin in an alkali-activated cementless binder led to a reduction in CO_2 emissions to 444 kg/ton, representing a 49.5 % decrease compared to OPC and a 2.2 % reduction compared to the 2-reference sample.

Fig. 13 and Appendix A compare the effect of OPC, 2 reference, and 2BMW40 based samples on the various environmental parameters. Notably, the performance of environmental such as climate change, photochemical oxidation, marine eutrophication, terrestrial acidification, and land occupation was significantly improved. However, the developed binder lacked in environmental indicators such as mineral resource use, Ozone layer depletion, and human toxicity. The inferior performance of the developed binder in comparison to the OPC relates to the use of chemicals in the form of alkali, the use of minerals in the form of metakaolin, and the use of energy in the treatment process of WCP, which can be further improved by optimizing these parameters in future studies.

5. Conclusion

In this study, the effect of BMWCP (burned milled waste concrete powder) and MWCP (milled waste concrete powder) on metakaolin based geopolymer binder with two different ratios of sodium silicate solution to sodium hydroxide was investigated. The mechanical and

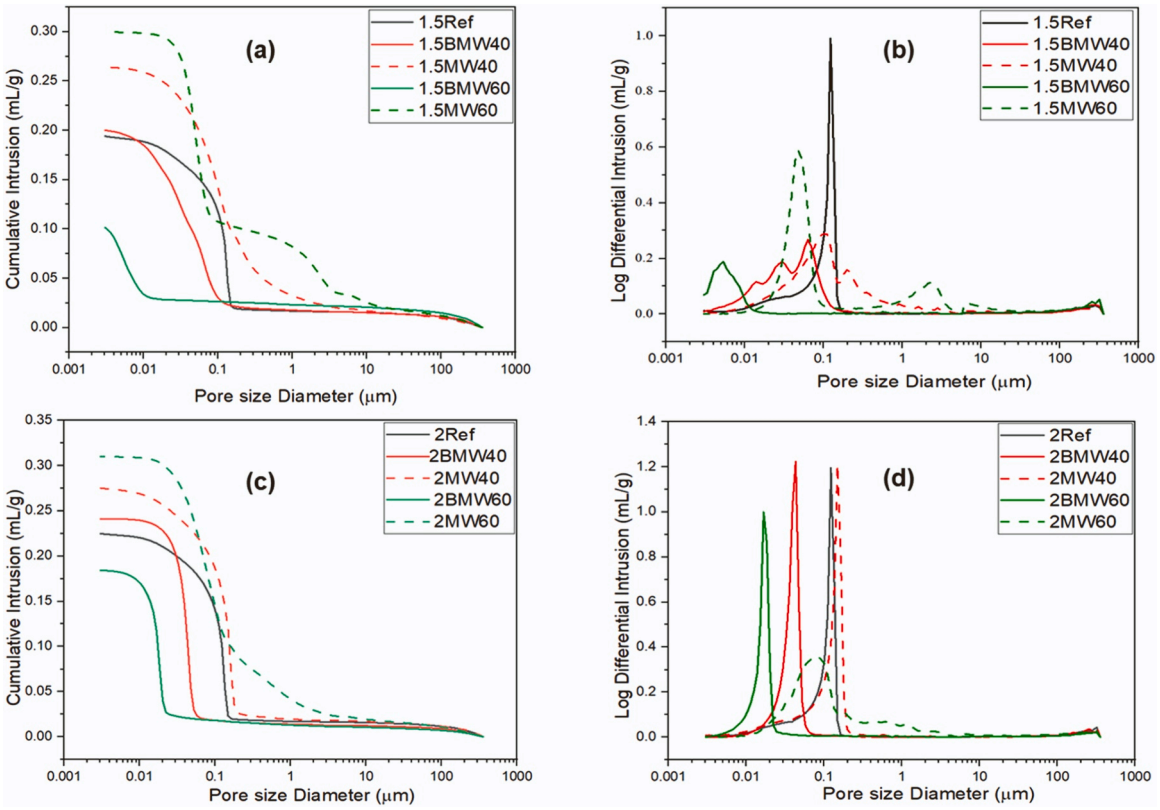

Fig. 11. MIP results samples with various alkali ratios, (a) pore size distribution with SSS/NH ratio of 1.5 (b) cumulative pore volume with SSS/NH ratio of 1.5 (c) pore size distribution with SSS/NH ratio of 2 (d) cumulative pore volume with SSS/NH ratio of 2.

Table 5
Total porosity and average pore diameter of the samples.

SSS/NH	1.5	2	1.5				2			
Sample Name	**Ref**		**BMW40**	**MW40**	**BMW60**	**MW60**	**BMW40**	**MW40**	**BMW60**	**MW60**
Average pore diameter (nm)	51.5	58.5	26.3	60.7	7.7	63.5	37.7	61.2	16.9	72.7
Total porosity (%)	27.7	31.0	29.7	34.6	17.8	39.1	33.7	35.3	29.0	39.5

chemical properties of the developed binder were assessed by using Chapelle test, compressive strength, XRD, FTIR, and MIP. Moreover, a life cycle assessment was conducted to comprehend the impact of alkali-activated WCP on the environment by comparing the newly developed binder to the metakaolin and OPC based binders. The summarized findings of this study are as following:

i) BMWCP consumed 24 % more lime compared to WCP and 10.5 % more lime than MWCP. The higher consumption of lime in BMWCP can be attributed to the presence of reactive silica, as confirmed by the Chappelle test. These findings establish BMWCP as the top consumer of lime among the three materials.
ii) BMWCP exhibited a superior compressive strength performance, for instance, an SSS/NH ratio of 1.5 only increased the strength by up to 20 % replacement of BMWCP, while an SSS/NH ratio of 2 performed better in high BMWCP content, especially 2BMWPC40, which demonstrated 61.7 % more compressive strength than that of the reference sample. This was due to the availability of more soluble silica and the reactive calcium in the matrix which promoted the development of the geopolymeric gel and C-S-H gel as the TGA and XRD support the decomposition of these phases.
iii) The development of more geopolymer gel and C-S-H gel in the case of 2BMW40 was also confirmed with isothermal calorimetry. The 2BMW40 evolved 33.8 % more cumulative heat than the reference sample. This outcome was also supported by FTIR analysis with higher wave number shifting of Si-O bond in the case of 2BMW40 mixture.
iv) The mixtures paste with BMWCP developed less porosity than other mixtures due to the formation of geopolymer gel and C-S-H gel. In the case of 2BMWCP40 generated 4.4 % less porosity than that of the 2MWCP40. Meanwhile, the increase in SSS/NH ratio develops more porosity due to the alkaline hydrolysis-induced dissolution of solid aluminosilicate as confirmed in the MIP analyses.
v) The climate change indicator of the binder prepared with BMWCP, namely 2BMW40 emitted 444 kg CO_2 eq/ton. This emission showed a reduction of 49.5 % in comparison to OPC and a reduction of 2.2 % in comparison to the reference mixture.

The activated WCP was used with metakaolin as a precursor in an alkali-activated binder which resulted in better strength properties, hydration properties, and porosity in mixture 2BMW40. The future goal of this research is to further reduce natural mineral use by increasing the recycled wastes and minimize/optimize the use of chemical activators with the consideration of their impacts on the setting time in the WCP based alkali-activated binder development process.

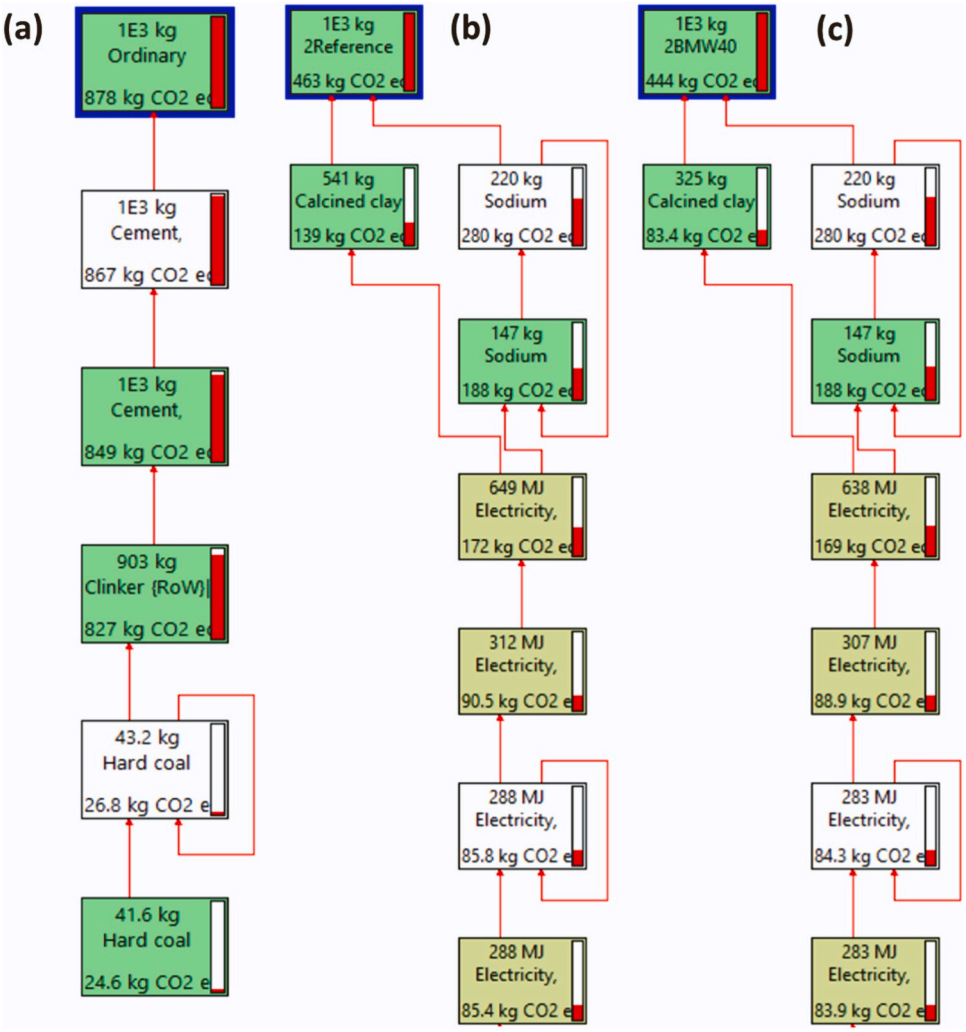

Fig. 12. The carbon dioxide emission of the different samples flow chart (a) OPC, (b) 2Reference, (c) 2BMW40.

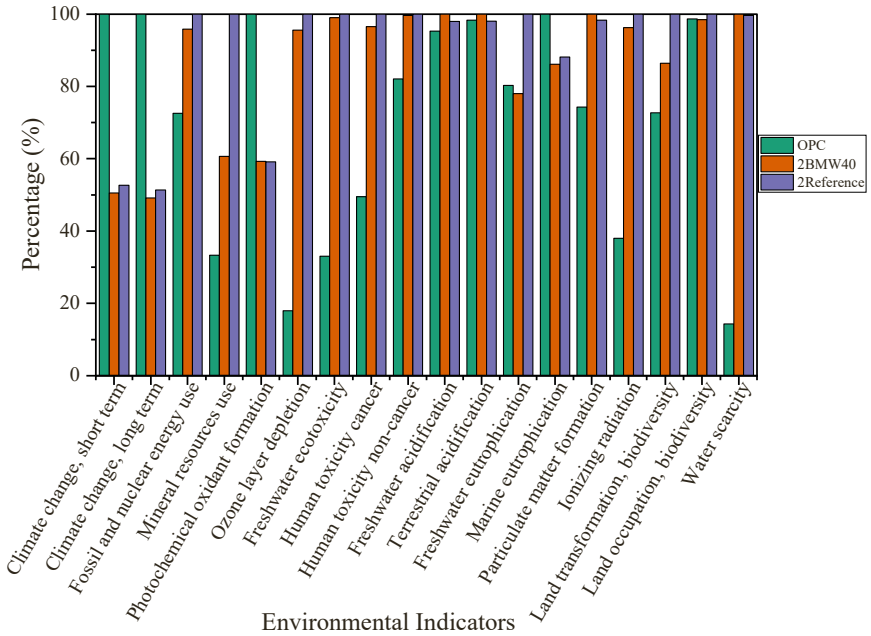

Fig. 13. Environmental impact assessment of OPC, 2Reference, 2BMW40.

CRediT authorship contribution statement

Sukhoon Pyo: Writing – review & editing, Supervision, Resources, Project administration, Methodology, Funding acquisition. **Martin Cyr:** Writing – review & editing, Supervision, Methodology, Formal analysis, Conceptualization. **Yanchen Oinam:** Writing – review & editing, Investigation, Formal analysis, Data curation. **Prabhat Vashistha:** Writing – review & editing, Validation, Methodology, Formal analysis, Conceptualization. **Aidarus Yonis:** Writing – original draft, Visualization, Methodology, Investigation, Formal analysis, Data curation.

Declaration of Competing Interest

The authors declare that they have no known competing financial interests or personal relationships that could have appeared to influence the work reported in this paper.

Data availability

Data will be made available on request.

Acknowledgement

This work was supported by the National Research Foundation of Korea (NRF) grant funded by the Korea government (MSIT) (No. RS-2023-00212366 and RS-2024-00399324). The opinions expressed in this paper are those of the authors and do not necessarily reflect the views of the sponsors or their employers.

Appendix A. Comparing the environmental impact per ton of WCP-based binder to that of OPC and Geopolymer-based binders

Label	Ordinary Portland Cement (%)	2BMW40 (%)	2Reference (%)
Climate change, short term	100	50.5045	52.6935
Climate change, long term	100	49.1324	51.371
Fossil and nuclear energy use	72.5845	95.8713	100
Mineral resources use	33.2909	60.6447	100
Photochemical oxidant formation	100	59.2355	59.096
Ozone layer depletion	17.9208	95.5784	100
Freshwater ecotoxicity	33.0508	99.0289	100
Human toxicity cancer	49.4892	96.564	100
Human toxicity non-cancer	82.1175	99.6305	100
Freshwater acidification	95.2717	100	97.9569
Terrestrial acidification	98.3674	100	98.0598
Freshwater eutrophication	80.3101	77.9787	100
Marine eutrophication	100	86.1482	88.141
Particulate matter formation	74.2488	100	98.3628
Ionizing radiation	38.0085	96.2535	100
Land transformation, biodiversity	72.7188	86.372	100
Land occupation, biodiversity	98.699	98.4726	100
Water scarcity	14.3014	100	99.6482

References

[1] M.H. Baghban, R. Mahjoub, Natural kenaf fiber and LC3 binder for sustainable fiber-reinforced cementitious composite: a review, Appl. Sci. 10 (1) (2020) 357.
[2] S.-C. Kou, C.-S. Poon, Properties of concrete prepared with crushed fine stone, furnace bottom ash and fine recycled aggregate as fine aggregates, Constr. Build. Mater. 23 (8) (2009) 2877–2886.
[3] J. Bhavsar, V.R. Panchal, Strength and durability evaluation of multi-binder geopolymer concrete in ambient condition, KSCE J. Civ. Eng. 27 (4) (2023) 1708–1719.
[4] T. Babu, S. Thangaraj, A novel approach for the synthesis of eco-friendly geopolymer ternary blended mortar with GGBS, sugarcane bagasse ash, and sewage sludge ash under ambient curing conditions, KSCE J. Civ. Eng. 27 (8) (2023) 3441–3454.
[5] M. Mansourghanaei, M. Biklaryan, A. Mardookhpour, Durability and mechanical properties of granulated blast furnace slag based geopolymer concrete containing polyolefin fibers and nano silica, KSCE J. Civ. Eng. 28 (1) (2024) 209–219.
[6] S. Kaza, et al., Urban Development;. ©. What a Waste 2.0: A Global Snapshot of Solid Waste Management to 2050., World Bank, Washington, DC, 2018.
[7] T.H.N. Rashidul Islam, A.S.M. Adhi Yuniarto, Uddin Shanawaz, Salmiati Salmiati, Shahid Shamsuddin, An empirical study of construction and demolition waste generation and implication of recycling, Waste Manag. 95 (2019) 10–21.
[8] J. Xiao, et al., Mechanical properties of concrete mixed with recycled powder produced from construction and demolition waste, J. Clean. Prod. 188 (2018) 720–731.
[9] P. Vashistha, S. Park, S. Pyo, A review on sustainable fabrication of futuristic cementitious binders based on application of waste concrete powder, steel slags, and coal bottom ash, Int. J. Concr. Struct. Mater. 16 (1) (2022) 1–28.
[10] P. Shen, et al., Synthesis of amorphous nano-silica from recycled concrete fines by two-step wet carbonation, Cem. Concr. Res. 147 (2021) 106526.
[11] Y. Huashan, C. Yujun, Influences of waste concrete powder on the strength development and hydration products of mortar containing fly ash, Mater. Sci. (2021).
[12] P. Vashistha, et al., Effect of thermo-mechanical activation of waste concrete powder (WCP) on the characteristics of cement mixtures, Constr. Build. Mater. 362 (2023) 129713.
[13] Y.J. Kim, Y.W. Choi, Utilization of waste concrete powder as a substitution material for cement, Constr. Build. Mater. 30 (2012) 500–504.
[14] Z. Ma, et al., Chloride permeability of concrete mixed with activity recycled powder obtained from C&D waste, Constr. Build. Mater. 199 (2019) 652–663.
[15] P. Shen, et al., Phase assemblance evolution during wet carbonation of recycled concrete fines, Cem. Concr. Res. 154 (2022) 106733.
[16] P. Vashistha, Y. Oinam, S. Pyo, Valorization of waste concrete powder (WCP) through silica fume incorporation to enhance the reactivity and hydration characteristics, Dev. Built Environ. (2023) 100272.
[17] M. Frías, et al., Reactivity in cement pastes bearing fine fraction concrete and glass from construction and demolition waste: Microstructural analysis of viability, Cem. Concr. Res. 148 (2021) 106531.
[18] H. Wu, et al., Utilizing thermal activation treatment to improve the properties of waste cementitious powder and its newmade cementitious materials, J. Clean. Prod. 322 (2021) 129074.
[19] Y. Sui, et al., Study on properties of waste concrete powder by thermal treatment and application in mortar, Appl. Sci. 10 (3) (2020) 998.
[20] S. Sasui, et al., Incorporation of waste glass as an activator in Class-C Fly Ash/GGBS based Alkali activated material, Materials 13 (17) (2020) 3906.
[21] S. Sasui, et al., Alkali activation of waste concrete powder: Effects of alkali type and concentration, Ceram. Int. 49 (10) (2023) 16260–16271.
[22] Zhi-hai, et al., A novel development of green UHPC containing waste concrete powder derived from construction and demolition waste, Powder Technol. 398 (2022) 117075.
[23] B. Lee, et al., Strength development properties of geopolymer paste and mortar with respect to amorphous Si/Al ratio of fly ash, Constr. Build. Mater. 151 (2017) 512–519.
[24] H.A. Abdel-Gawwad, M.S. Mohammed, S.E. Zakey, Preparation, performance, and stability of alkali-activated-concrete waste-lead-bearing sludge composites, J. Clean. Prod. 259 (2020) 120924.
[25] C.G. Oscar Mendoza, S.Camargo Sergio, I.Tobón Jorge, Structural and nano-mechanical properties of Calcium Silicate Hydrate (C-S-H) formed from alite

hydration in the presence of sodium and potassium hydroxide, Cem. Concr. Res. 74 (2015) 88–94.
[26] G.S. Aditya Kumar, Patapy Cedric, Gianocca Caterina, L.Scrivener Karen, The influence of sodium and potassium hydroxide on alite hydration: experiments and simulations, Cem. Concr. Res. 42 (11) (2012) 1513–1523.
[27] H. Abdel-Gawwad, et al., Recycling of concrete waste to produce ready-mix alkali activated cement, Ceram. Int. 44 (6) (2018) 7300–7304.
[28] W. Chen, Z. Zhu, Synthesis and characterization of metakaolin modified waste concrete-based geopolymer, in: *Proceedings of the 2nd International Symposium on Asia Urban GeoEngineering*, Springer, 2018.
[29] S.Lee Kyo, et al., Mineralogical characteristics and physico-chemical properties of a newly reclaimed tidal flat of haenam bay in the southwestern coast of korea, Korean J. Soil Sci. Fertil. 52 (2019) 475–488.
[30] M.J. Sabzoi Nizamuddin, Gravina Rebecca, Giustozzi Filippo, Recycled plastic as bitumen modifier: the role of recycled linear low-density polyethylene in the modification of physical, chemical and rheological properties of bitumen, J. Clean. Prod. 266 (2020) 121988.
[31] D.C.B. Misael Cardona, S. Gregory, Patience, Thermogravimetric heat and mass transfer: modeling of bitumen pyrolysis, Fuel 143 (2015) 253–261.
[32] S. Singh, P. Vashistha, Development of newer composite cement through mechano-chemical activation of steel slag, Constr. Build. Mater. 268 (2021) 121147.
[33] NF, P., *P 18 -513*: *Pozzolanic addition for concrete–Metakaolin—Definitions, specifications and conformity criteria.* Association Française de Normalisation, Saint-Denis, 2010.
[34] K. Scrivener, R. Snellings, B. Lothenbach, A practical guide to microstructural analysis of cementitious materials, Vol. 540, Crc Press, Boca Raton, FL, USA, 2016.
[35] ASTM, Stand. Test. Method Meas. Heat. hydration Hydraul. Cem. Mater. Using isothermal Conduct. Calorim. (2009).
[36] Y. Luo, H.J. H.B, Qingliang Yu, Understanding the gel compatibility and thermal behavior of alkali activated Class F fly ash/ladle slag: the underlying role of Ca availability, Cem. Concr. Res. 170 (2023).
[37] Oinam Yanchen, K.A.M, Vashistha Prabhat, Pyo Sukhoon, Utilization of paper mill lime mud to partially replace fillers in cementless ultra-high performance concrete (UHPC), Constr. Build. Mater. 426 (2024) 136177.
[38] IEA, World Energy Balances. 2019, OECD Publishing: Paris.
[39] Md Luxan, F. Madruga, J. Saavedra, Rapid evaluation of pozzolanic activity of natural products by conductivity measurement, Cem. Concr. Res. 19 (1) (1989) 63–68.
[40] A.M. Kaja, A.L, Q.L. Yu, Effects of Portland cement on activation mechanism of class F fly ash geopolymer cured under ambient conditions, Constr. Build. Mater. 189 (2018) 1113–1123.
[41] K.-L.L. Kang Gao, DeYing Wang, Chao-Lung Hwang, Hau-Shing Shiu, Yu-Min Chang, Ta-Wui Cheng, Effects SiO2/Na2O molar ratio on mechanical properties and the microstructure of nano-SiO2 metakaolin-based geopolymers, Constr. Build. Mater. 53 (2014) 503–510.
[42] P. De Silva, K. S.-C, V. Sirivivatnanon, Kinetics of geopolymerization: role of Al2O3 and SiO2, Cem. Concr. Res. 37 (2007) 512–518.
[43] F. Pacheco-Torgal, J. Castro-Gomes, S. Jalali, Properties of tungsten mine waste geopolymeric binder, Constr. Build. Mater. 22 (2008) 1201–1211.
[44] P. Duxson, et al., Geopolymer technology: the current state of the art, J. Mater. Sci. 42 (9) (2007) 2917–2933.
[45] C.K. Yip, G. Lukey, J.S. Van Deventer, The coexistence of geopolymeric gel and calcium silicate hydrate at the early stage of alkaline activation, Cem. Concr. Res. 35 (9) (2005) 1688–1697.
[46] I. Lecomte, et al., Micro)-structural comparison between geopolymers, alkali-activated slag cement and Portland cement, J. Eur. Ceram. Soc. 26 (16) (2006) 3789–3797.
[47] J. Van Deventer, et al., Reaction mechanisms in the geopolymeric conversion of inorganic waste to useful products, J. Hazard. Mater. 139 (3) (2007) 506–513.
[48] W. Lee, J. Van Deventer, The effect of ionic contaminants on the early-age properties of alkali-activated fly ash-based cements, Cem. Concr. Res. 32 (4) (2002) 577–584.
[49] J. Temuujin, A. Van Riessen, R. Williams, Influence of calcium compounds on the mechanical properties of fly ash geopolymer pastes, J. Hazard. Mater. 167 (1-3) (2009) 82–88.
[50] F. Pacheco-Torgal, J. Castro-Gomes, S. Jalali, Investigations on mix design of tungsten mine waste geopolymeric binder, Constr. Build. Mater. 22 (9) (2008) 1939–1949.
[51] X.R. Saeed Ahmari, Toufigh Vahab, Zhang Lianyang, Production of geopolymeric binder from blended waste concrete powder and fly ash, Constr. Build. Mater. 35 (2012) 718–729.
[52] Christina K. Yip, G.C.L, L.Provis John, Jannie S.J. van Deventer, Effect of calcium silicate sources on geopolymerisation, Cem. Concr. Res. 38 (2008) 554–564.
[53] B. Mota, T.M, K. Scrivener, Impact of NaOH and Na2SO4 on the kinetics and microstructural development of white cement hydration, Cem. Concr. Res. 108 (2018) 172–185.
[54] K.A.M. Sungwoo Park, Wu Siyu, Pyo Sukhoon, Characteristics of hybrid alkaline cement composites with high cement content: flash set and high compressive strength, J. Mater. Res. Technol. 17 (2022) 1582–1597.
[55] P. Vashistha, K.A. Moges, S. Pyo, Alkali activation of paper industry lime mud and assessment of its application in cementless binder, Dev. Built Environ. (2023) 100146.
[56] C.K. Yip, G.C. Lukey, J.S.J. Van Deventer, The coexistence of geopolymeric gel and calcium silicate hydrate at the early stage of alkaline activation, Cem. Concr. Res. 35 (9) (2005) 1688–1697.
[57] Buchwald, A, H. Hilbig, C. Kaps, Alkali-activated metakaolin-slag blends - performance and structure in dependence of their composition, J. Mater. Sci. 42 (9) (2007) 3024–3032.
[58] K. Dombrowski, A. Buchwald, M. Weil, The influence of calcium content on the structure and thermal performance of fly ash based geopolymers, J. Mater. Sci. 42 (9) (2007) 3033–3043.
[59] J.E. Oh, et al., The evolution of strength and crystalline phases for alkali-activated ground blast furnace slag and fly ash-based geopolymers, Cem. Concr. Res. 40 (2) (2010) 189–196.
[60] F. Pacheco-Torgal, J.P. Castro-Gomes, S. Jalali, Investigations of tungsten mine waste geopolymeric binder: strength and microstructure, Constr. Build. Mater. 22 (11) (2008) 2212–2219.
[61] K.J.D. MacKenzie, M.E. Smith, A. Wong, A multinuclear MAS NMR study of calcium-containing aluminosilicate inorganic polymers, J. Mater. Chem. 17 (48) (2007) 5090–5096.
[62] S. Ahmari, et al., Production of geopolymeric binder from blended waste concrete powder and fly ash, Constr. Build. Mater. 35 (2012) 718–729.
[63] O.A. Abdulkareem, et al., Effects of elevated temperatures on the thermal behavior and mechanical performance of fly ash geopolymer paste, mortar and lightweight concrete, Constr. Build. Mater. 50 (2014) 377–387.
[64] A.F.-J. García-Lodeiro, A. Palomo, Variation in hybrid cements over time. Alkaline activation of fly ash–portland cement blends, Cem. Concr. Res. 52 (2013).
[65] P. Vashistha, S. Park, S. Pyo, A review on sustainable fabrication of futuristic cementitious binders based on application of waste concrete powder, steel slags, and coal bottom ash, Int. J. Concr. Struct. Mater. 16 (1) (2022) 51.
[66] Oksri-Nelfia, et al., Reuse of recycled crushed concrete fines as mineral addition in cementitious materials, Mater. Struct. 49 (2016) 3239–3251.
[67] M. Liu, et al., Microstructure and macro properties of sustainable alkali-activated fly ash mortar with various construction waste fines as binder replacement up to 100, Cem. Concr. Compos. 134 (2022) 104733.
[68] Z. Sun, A. Vollpracht, Isothermal calorimetry and in-situ XRD study of the NaOH activated fly ash, metakaolin and slag, Cem. Concr. Res. 103 (2018) 110–122.
[69] X. Yao, et al., Geopolymerization process of alkali-metakaolinite characterized by isothermal calorimetry, Thermochim. Acta 493 (1-2) (2009) 49–54.
[70] N. Clayden, et al., Solid state 27Al NMR and FTIR study of lanthanum aluminosilicate glasses, J. Non-Cryst. Solids 258 (1-3) (1999) 11–19.
[71] N. Lee, H.-K. Lee, Reactivity and reaction products of alkali-activated, fly ash/slag paste, Constr. Build. Mater. 81 (2015) 303–312.
[72] H. El-Didamony, et al., Effect of substitution of granulated slag by air-cooled slag on the properties of alkali activated slag, Ceram. Int. 39 (1) (2013) 171–181.
[73] A. Allahverdi, E. Najafi Kani, Construction wastes as raw materials for geopolymer binders, Int. J. Civ. Eng. 7 (3) (2009) 154–160.
[74] W.K.W. Lee, J.S.J. Van Deventer, Use of infrared spectroscopy to study geopolymerization of heterogeneous amorphous aluminosilicates, Langmuir 19 (21) (2003) 8726–8734.
[75] I. Giannopoulou, et al., Utilization of metallurgical solid by-products for the development of inorganic polymeric construction materials, Glob. Nest J. 11 (2) (2009) 127–136.
[76] Sasui Sasui, G.K, Arie van Riessen, Syed Fakhar Alam, Jeongsoo Nam, Shafiq Ishak, Hamin Eu, Influence of elevated temperature on waste concrete powder and its application in alkali activated materials, J. Clean. Prod. 434 (2024) 140423.
[77] Y. Zhang, W. Sun, Z. Li, Infrared spectroscopy study of structural nature of geopolymeric products, J. Wuhan. Univ. Technol. -Mater. Sci. Ed. 23 (4) (2008) 522–527.
[78] L. Fernández-Carrasco, et al., Infrared spectroscopy in the analysis of building and construction materials, Infrared Spectrosc. –Mater. Sci. Eng. Technol. 510 (2012).
[79] S. Cui, et al., Experimental study on mechanical property and pore structure of concrete for shotcrete use in a hot-dry environment of high geothermal tunnels, Constr. Build. Mater. 173 (2018) 124–135.
[80] M. Anwar, D.A. Emarah, Pore structure of concrete containing ternary cementitious blends, Results Mater. 1 (2019) 100019.
[81] C. Li, et al., Pore structure and permeability of concrete with high volume of limestone powder addition, Powder Technol. 338 (2018) 416–424.
[82] F.G.M. Aredes, et al., Effect of cure temperature on the formation of metakaolinite-based geopolymer, Ceram. Int. 41 (6) (2015) 7302–7311.
[83] J.S.J. Van Deventer, J.L. Provis, P. Duxson, Technical and commercial progress in the adoption of geopolymer cement, Miner. Eng. 29 (2012) 89–104.
[84] Y. Zhao, et al., The particle-size effect of waste clay brick powder on its pozzolanic activity and properties of blended cement, J. Clean. Prod. 242 (2020) 118521.
[85] J. Shao, et al., Study on the pozzolanic reaction of clay brick powder in blended cement pastes, Constr. Build. Mater. 213 (2019) 209–215.
[86] M. O'Farrell, S. Wild, B. Sabir, Pore size distribution and compressive strength of waste clay brick mortar, Cem. Concr. Compos. 23 (1) (2001) 81–91.
[87] R.H. Sadok, et al., Life cycle assessment of cementitious materials based on calcined sediments from Chorfa II dam for low carbon binders as sustainable building materials, Sci. Total Environ. 826 (2022) 154077.